Supporting Information

Silva-Ayala et al. 10.1073/pnas.1304932110

SI Materials and Methods

Cells and Viruses. Monkey kidney MA104 cells, of *Cercopithecus aethiops* epithelial kidney origin, were grown in advanced DMEM supplemented with 4.5% FBS. Human intestinal epithelial (Caco-2) cells (clone C2Bb1) of human intestinal origin were grown in high-glucose DMEM supplemented with 10% FBS and nonessential amino acids. Rhesus rotavirus (RRV) and rotavirus (RV) human strains Wa and DS-1 were obtained from H. B. Greenberg (Stanford University, Stanford, CA) and were propagated in MA104 cells as described previously (1). Human species C adenovirus serotype 5 (Ad5) was propagated in HeLa cells and was kindly provided by Ramón González (Morelos State University, Cuernavaca, Morelos, Mexico). Rotavirus lysates were activated with trypsin (10 μg/mL; GibcoBRL) for 30 min at 37 °C. Rotavirus double-layered particles (DLPs) and triple-layered particle (TLPs) were purified by cesium chloride (CsCl) density gradients, as reported (1).

Plasmids, Antibodies, Primers, and Reagents. mAbs to rotaviral proteins VP5 (2G4) and VP7 (159) were kindly provided by H. B. Greenberg (Stanford University, Stanford, CA). Rabbit polyclonal sera to rotavirus structural proteins (anti-TLPs) and to the rotavirus nonstructural protein NSP5 were produced in our laboratory. Mouse mAb 6C4 anti-lysobisphosphatidic acid (LBPA) was purchased from Echelon. Mouse mAb specific for the DBP protein of human adenovirus 5 (Adv5) was kindly provided by Ramón González (Morelos State University, Cuernavaca, Mexico) (2). mAbs to small GTPases RAB5 and RAB7 were obtained from Cell Signaling. The secondary antibodies used were goat anti-rabbit or anti-mouse coupled to Alexa Fluor-488, -568, or -647 (Molecular Probes) or to IRDye 800 (LI-COR Biosciences). Horseradish peroxidase-conjugated goat anti-rabbit polyclonal antibody was from Perkin-Elmer Life Sciences. Plasmids pCR3.1/YFP/Tsg101, pCR3.1/GFP/Tsg101/1–157, pCR3.1/CFP/VPS4AA, pCR3.1/CFP/VPS4AAE228Q, pCR3.1/YFP/Alix, pCR3.1/YFP/Alix 176–869, and pCR3.1/CFP/HRS were kindly provided by P. D. Bieniasz (Rockefeller University, New York) (3). Plasmids expressing RAB5Q79L, RAB5S534N, RAB7, and RAB7NI25I proteins were provided by J. Gruenberg (University of Geneva). Expression plasmids for small GTPases CDC42, CDC42N17, and CDC42V12 were a gift from F. Sánchez (Universidad Autónoma de Madrid, Madrid). Transferrin (Tf) labeled with Alexa 594 was purchased from Molecular Probes. Alexa Fluor 680-succinimidyl ester (Invitrogen) was used for total protein detection in the RNAi screen.

Infectivity Assays and Immunofluorescence. MA104 cells grown on glass coverslips were transfected with the indicated plasmids or with siRNA as previously described (4). Cells were then infected with RRV at a multiplicity of infection (MOI) of 3 or 5 for 1 h at 37 °C or transfected with 500 ng of DLPs at 24–48 h post-transfection (hpt) (for plasmids) or at 72 hpt (for siRNAs). At 6 hpi, cells were fixed with 2% formaldehyde for 20 min at room temperature (RT) and permeabilized by incubation with 0.5% Triton X-100 in blocking buffer (1% BSA diluted in PBS) for 15 min. Primary (anti-NSP5 or anti-TLPs) and secondary antibodies were incubated for 1 h at RT in blocking buffer. Coverslips were mounted on glass slides using Fluokeep (Argene), and the samples were observed under a fluorescence microscope (Zeiss, Axioskop 2) coupled to a digital camera (Photometrics Cool Snap HQ). Colocalization of cellular proteins and viral particles was visualized using a Bio-Rad MRC confocal microscope, coupled to an Axiophot camera (Zeiss), or using a Zeiss LSM 510 meta confocal microscope. Each colocalization was performed in triplicate, and five randomly selected cells per time point per experiment were analyzed with ImageJ 1.45S software using a colocalization plugin, and quantification of the signal was made with a threshold of 0.03–1.3 μm^2. In plasmid transfection assays, only the cells expressing the plasmid-encoded protein were scored, and the relative infectivity of cells expressing the mutant proteins was calculated by normalizing against cells expressing the wild-type protein. The effect of the dominant-negative (DN) mutants in Caco-2 cells could not be tested on the infectivity of Wa and DS-1 viruses because the infectious titer of these two viruses in this cell line is on the order of 10^4 pfu/mL, about 10- to 20-fold lower than that obtained in MA104 cells. The low virus infectivity combined with the low transfection efficiency of plasmids did not allow us to have enough simultaneously transfected and infected cells to evaluate the effect of the DN proteins on virus infectivity. For the Adv5 infectivity assay, MA104 cells were infected at an MOI of 10 for 1 h at 37 °C. Virus was washed away, and cells were incubated for 20 h at 37 °C in DMEM 5% FBS. Cells were prepared for immunofluorescence as described and incubated with a mAb to the adenoviral protein DBP.

Enrichment Analyses. The classification of genes into biological functions and pathways was made using the Ingenuity Systems software online (www.ingenuity.com, Table S2). The enrichment or overrepresentation for the set of hits within each category relative to the whole set of genes tested in the RNAi screen was calculated using the statistical tool *P* value, which is computed using the hypergeometric probability distribution implemented in the R language.

Real-Time PCR. To quantify the knockdown efficiency of siRNAs by real-time RT-PCR, MA104 cells grown in 12-well plates transfected with siRNAs and infected with RRV as previously described were lysed with TRIzol, and total RNA was purified according to the manufacturer's instructions. Total RNA (100 ng) was used as template, and DNA amplification was made in the presence of a Sybergreen PCR master mix using an ABI Prism 700 detection system (Applied Biosystems). Viral negative-strand RNA was amplified using forward primers for the NSP4 gene, as described (5), and the C_T for each amplified RNA sample was calculated. The threshold cycle (ΔC_T) was used to calculate the relative fold changes in gene expression normalized against the GAPDH control (5).

Immunoblot Analysis. To quantify the silencing efficiency of siRNAs by Western blot, transfected and infected cells were lysed in Laemmli sample buffer, denatured by boiling for 5 min, subjected to SDS/PAGE, and transferred to Immobilon NC (Millipore) membranes. The membranes were blocked with tris-buffered saline or PBS containing 5% nonfat dry milk and incubated with the indicated antibodies. The bound antibodies were detected by incubation with a peroxidase-labeled secondary antibody and the Western Lightning system (Perkin-Elmer).

Anti-LBPA Antibody Treatment. MA104 cells were preincubated with 50 mg/mL of anti-LBPA antibody or with 50 mg/mL of isotype IgG control for 16 h and infected with RRV and Wa for 1 h at 4 °C in the absence of antibody; cells were washed twice and incubated at 37 °C in MEM.

Virus Cell Entry Analysis by Confocal Microscopy. This assay was carried out based on a previous report (6). Cells grown on glass coverslips were washed twice and incubated in MEM without serum for 30 min at 37 °C, and cells were then incubated with 0.5% BSA in PBS for 1 h at 4 °C. CsCl-purified RRV TLPs (MOI 50) were added and incubated for 1 h at 4 °C; unbound virus was removed by washing, and the cells were incubated in MEM at 37 °C for the indicated periods of time. The cells were then fixed, processed for IF, and analyzed by confocal microscopy as indicated in *Infectivity Assays and Immunofluorescence*.

Virus-Binding Assays. MA104 cells grown in 96-well plates were washed twice and incubated with MEM without serum for 30 min at 37 °C. After this, MEM was removed, and 200 μL of blocking solution (1% of BSA in PBS) was added to the cells, followed by incubation for 1 h at room temperature. Cells were then washed with an ice-cold solution of 0.5% BSA-PBS and incubated with 400 ng of RRV TLPs in blocking solution for 1 h at 4 °C. Cells were then washed three times with ice-cold 0.5% BSA-PBS, and 60 μL of lysis buffer [50 mM Tris·HCl (pH 7.5), 150 mM NaCl, 0.1% Triton X-100] was added. The cells were frozen and thawed twice, and the amount of virus present in the cell lysate was determined by an ELISA as described previously (7). A direct ELISA with increasing amounts of purified viruses was performed in parallel to quantify the virus.

Transferrin Uptake Assays. For analysis of the uptake of Tf, cells grown on coverslips transfected as described above were chilled on ice for 10 min and then incubated with 50 μg/mL of Alexa 594-Tf on ice for 30 min. The cells were washed twice with cold medium and then incubated at 37 °C in a CO_2 incubator for 30 min (4). At the end points of the assay the samples were fixed in 2% paraformaldehyde in PBS for 20 min and processed for IF as described above.

Statistical Analysis. For both screens the positive hits were defined as treatments that decreased more than 25% the normalized fluorescence intensity ratio (signal from mAb 2G4/signal from Alexa 680-succinimydil ester) compared with the negative control, irrelevant (Irr) siRNA, with a SD of less than 25% in the fluorescence ratio of the raw values. All statistical evaluations were carried out using a Mann–Whitney *t*-test and GraphPad Prism software.

1. Pando V, Isa P, Arias CF, López S (2002) Influence of calcium on the early steps of rotavirus infection. *Virology* 295(1):190–200.
2. Cardoso FM, Kato SE, Huang W, Flint SJ, Gonzalez RA (2008) An early function of the adenoviral E1B 55 kDa protein is required for the nuclear relocalization of the cellular p53 protein in adenovirus-infected normal human cells. *Virology* 378(2):339–346.
3. Martin-Serrano J, Zang T, Bieniasz PD (2003) Role of ESCRT-I in retroviral budding. *J Virol* 77(8):4794–4804.
4. Sánchez-San Martín C, López T, Arias CF, López S (2004) Characterization of rotavirus cell entry. *J Virol* 78(5):2310–2318.
5. Ayala-Breton C, et al. (2009) Analysis of the kinetics of transcription and replication of the rotavirus genome by RNA interference. *J Virol* 83(17):8819–8831.
6. Wolf M, Vo PT, Greenberg HB (2011) Rhesus rotavirus entry into a polarized epithelium is endocytosis dependent and involves sequential VP4 conformational changes. *J Virol* 85(6):2492–2503.
7. Zárate S, et al. (2000) Integrin alpha2beta1 mediates the cell attachment of the rotavirus neuraminidase-resistant variant nar3. *Virology* 278(1):50–54.

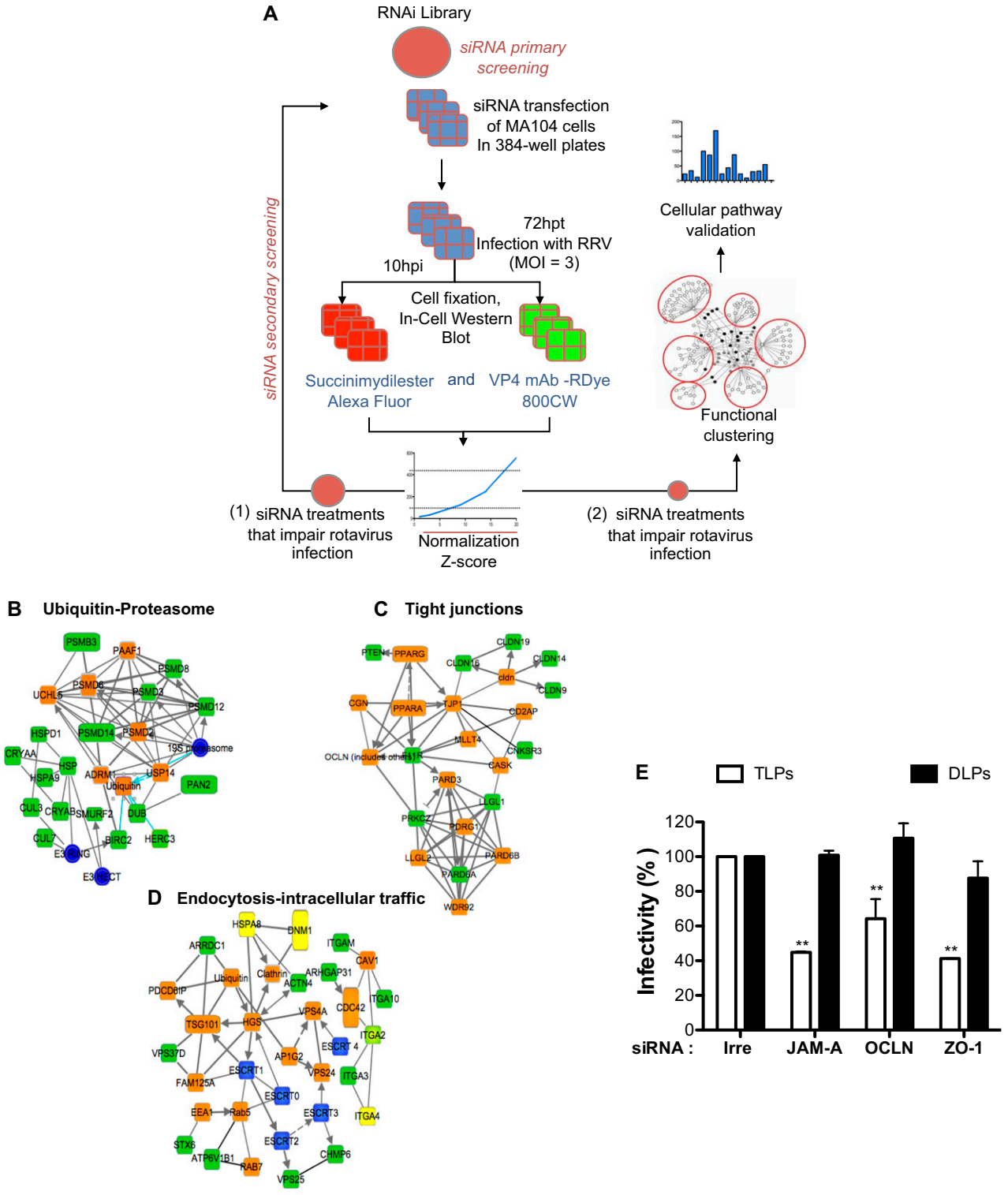

Fig. S1. Genome-wide screen identifies cellular factors required on rotavirus infection. (*A*) Outline of the genome-wide RNAi screen to identify host factors required for rotavirus infection. (*B–D*) Predicted interactions of positive hits. Interaction of (*B*) ubiquitin-proteasome, (*C*) tight junctions, and (*D*) endocytosis-intracellular traffic components, assessed using STRING, Ingenuity Systems, Panther, and David databases. Screen-positive hits are shown in green; characterized cellular proteins involved in rotavirus infection are in yellow; predicted positive hits in orange; blue circles indicate protein clusters with similar function. (*E*) Components of the tight junction network are involved in rotavirus infection. MA104 cells were transfected with the indicated siRNAs and at 72 hpt were either infected with RRV (MOI 3) or transfected with RRV DLPs. At 6 hpi, the cells were processed for immunofluorescence. Rotavirus infectivity was evaluated by the presence of viroplasms within the cell using an antibody against NSP5. The calculated virus infectivity was normalized against an irrelevant siRNA—in this case, an siRNA directed to the cellular protein GRP94. The resulting infectivity was normalized against that observed in cells transfected with an irrelevant siRNA. Data represent the arithmetic mean and SEM of three independent experiments. $^{**}P < 0.01$.

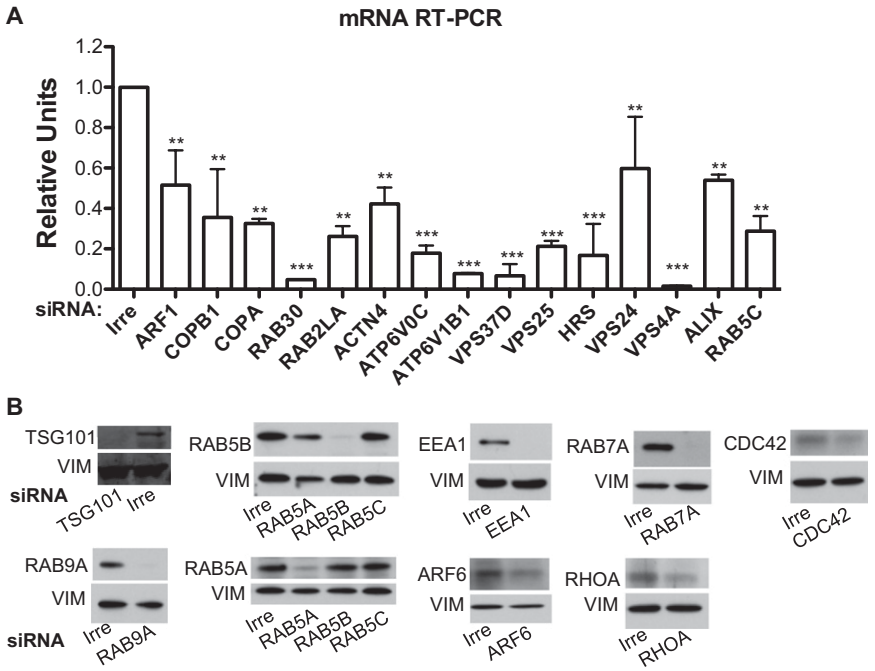

Fig. S2. Analysis of the siRNA efficiency. MA104 cells were transfected with the indicated siRNAs or with an irrelevant siRNA. The efficiency of silencing was assessed at 72 hpt by (*A*) quantification of the respective mRNA levels by quantitative RT-PCR or by (*B*) Western blot, as indicated in *SI Materials and Methods*. Data represent the arithmetic mean and SEM of three independent experiments. ***$P < 0.001$; **$P < 0.01$.

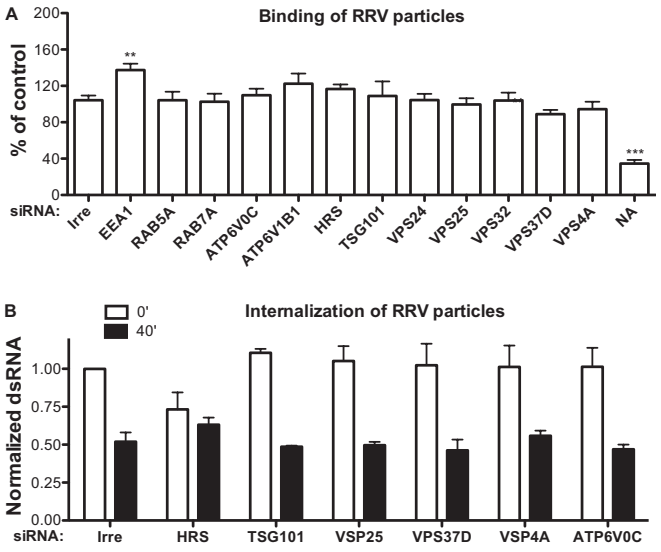

Fig. S3. Knocked-down expression of endosomal sorting complexes required for transport (ESCRT) and endocytosis-related components affects neither rotavirus binding nor internalization into the host cell. Cells were transfected with the indicated siRNAs and at 72 hpt were infected with purified RRV TLPs (MOI 50) and processed for binding assay or RT-PCR. (*A*) TLPs were incubated with MA104 cells for 1 h at 4 °C that had been transfected with the indicated siRNAs or previously treated with 10 mU/mL of *Arthrobacter ureafasciens* neuraminidase (NA) for 1 h at 37 °C. Binding assay was performed as indicated in *SI Materials and Methods*. Data are expressed as the percentage of the virus detected by ELISA in cells transfected with an irrelevant siRNA. (*B*) TLPs were incubated with MA104 cells for 1 h at 4 °C and then shifted to 37 °C. Viral particles present at the cell surface were removed with 3 mM EGTA at the indicated time points, the cells were lysed with TRIzol (Invitrogen), and the RNA was purified for RT-PCR. Data are expressed as the normalization of the NSP4 gene negative strand detected against GAPDH mRNA in cells transfected with an irrelevant siRNA. Data represent the arithmetic mean and SEM of three independent experiments. ***$P < 0.001$; **$P < 0.01$.

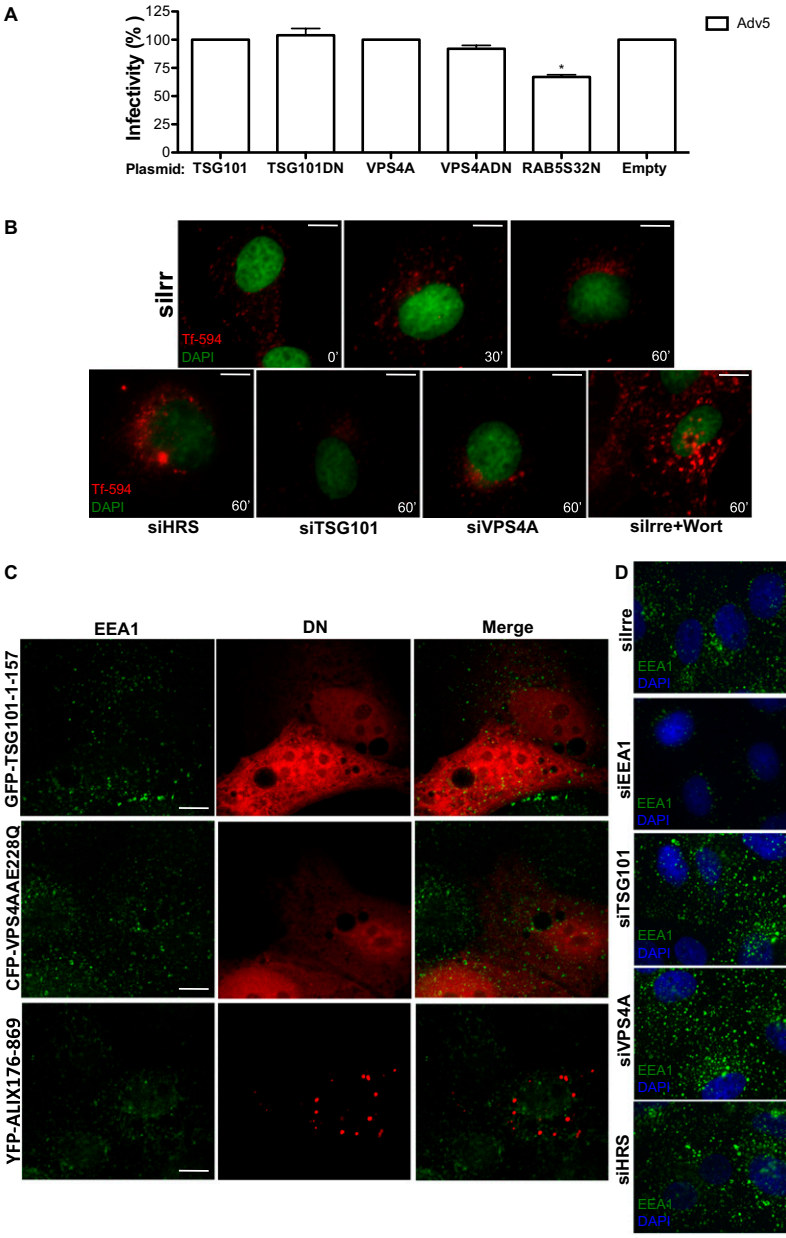

Fig. S4. Impairing the function of ESCRT components does not impair adenovirus replication, the integrity of endosomes, or transferring uptake. (*A*) MA104 cells were transfected with the indicated plasmids and infected with Adv5 as described in *SI Materials and Methods*. At 20 hpi, infected cells were fixed and processed for IF and analyzed. Adv5-infected cells were quantified by measuring the expression of viral protein DBP detected indirectly by an mAb. (*B*) MA104 cells transfected with the indicated siRNAs were incubated with Alexa 594-Tf as indicated in *SI Materials and Methods*. Cells were fixed at the indicated times and transferrin internalization was analyzed by confocal microscopy. Representative images are shown. MA104 cells were transfected with the indicated (*C*) plasmids or (*D*) siRNAs. At 24 and 72 hpt, respectively, cells were processed for immunofluorescence and analyzed by confocal microscopy. Endosome integrity was evaluated by the presence of the early endosomal antigen 1 (EEA1) protein clusters in cells expressing the indicated fluorescent-ESCRT proteins. For EE detection, a mAb against EEA1 was used; Alexa-488, -568, or -467 was used as secondary antibody. Representative images are shown. [Scale bars: (*B* and *C*) 5 μm and (*D*) 10 μm.]

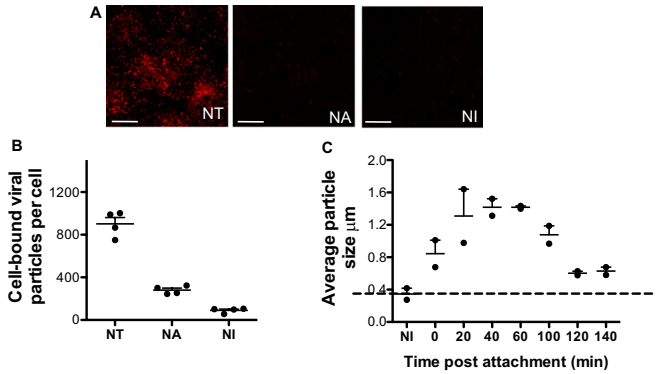

Fig. S5. Identification of rotavirus particles by confocal microscopy. (*A*) Purified RRV TLPs (MOI 50) were incubated with MA104 cells for 1 h at 4 °C; these cells had been previously treated with 10 mU/mL of *A. ureafasciens* neuraminidase (NA) for 1 h at 37 °C. The cells were fixed and immunostained under non-permeabilizing conditions as described in *SI Materials and Methods*. Viral particles were detected indirectly using anti-TLPs as primary antibodies and Alexa-568 as secondary antibody. Representative images are shown. (Scale bars, 5 μM.) NT, nontreated cells; NA, neuraminidase-treated cells; NI, not infected. (*B*) Viral particles were detected indirectly using anti-TLP antibodies and quantified in three different experiments by confocal microscopy. (*C*) Purified RRV TLPs were incubated with MA104 cells (MOI 50) for 1 h at 4 °C, quickly shifted at 37 °C, and analyzed by immunofluorescence and confocal microscopy at the indicated times. Viral particles were detected indirectly using anti-TLPs as primary antibodies and Alexa-568 as secondary antibody. Analysis of the immunofluorescent signal revealed a time-dependent significant increase in the average size of the signal associated with viral particles. Signal detection and quantification was made by confocal microscopy; five randomly selected cells per time point were analyzed, and viral particles were determined as described in *SI Materials and Methods*. Data represent the arithmetic mean and SEM of three independent experiments.

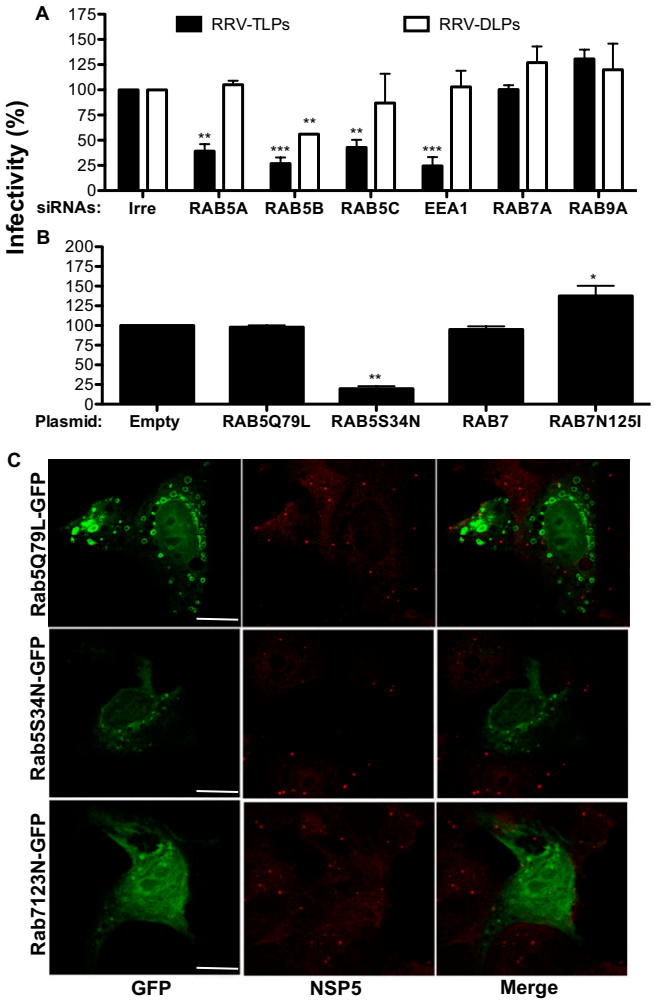

Fig. S6. RRV enters cells through an early endosome-dependent pathway. (*A*) MA104 cells were transfected with the indicated siRNAs and at 72 hpt were either infected with RRV (MOI 3) or transfected with RRV DLPs. (*B*) MA104 cells were transfected with the indicated plasmids, and at 24 hpt were infected with RRV (MOI 5). At 6 hpi, cells were fixed and processed for IF using anti-NSP5 antibodies to detect infected cells, as described in *SI Materials and Methods*. The infectivity is expressed as the percentage of that observed in cells transfected with an irrelevant siRNA (Irre). The relative infectivity of cells expressing DN-RAB7 was obtained by normalizing against its wild-type counterpart. (*C*) Representative images for DN-RAB expression are shown. (Scale bars, 10 μm.) The infectivity of DN-RAB5 was normalized against cells transfected with an empty plasmid. Data represent the arithmetic mean and SEM of three independent experiments. ***$P < 0.001$; **$P < 0.01$; *$P < 0.05$.

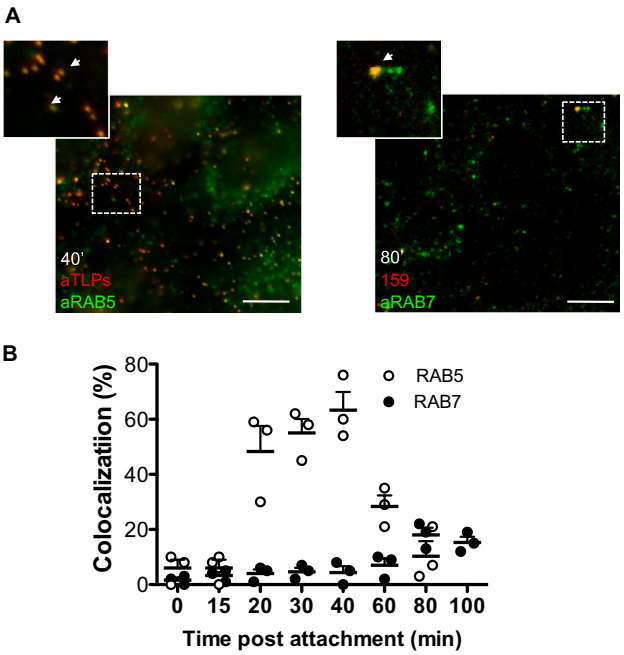

Fig. S7. Incoming RRV particles colocalize with RAB5 but not with RAB7. (*A*) MA104 cells were incubated for 1 h at 4 °C with purified RRV TLPs (MOI of 50) and quickly shifted to 37 °C for the indicated periods of time; the cells were fixed and processed for IF using either anti-TLPs antibodies in parallel with mAb to RAB5 or mAb 159 in parallel with polyclonal Ab to RAB7. (Scale bars, 5 μm.) (*B*) Quantification of viral particles was carried out by confocal microscopy analysis. The percentage of colocalization of RRV particles with RAB GTPases is shown relative to total RRV particles detected in each cell. Quantification of viral particles and determination of the colocalization events were done as described in the legend for Fig. 3.

Other Supporting Information Files

Table S1 (RTF)
Table S2 (RTF)

Table S1. Positive hits in the RNAi screening of cellular proteins required for rotavirus infection		
Protein	**Number of siRNAs tested**	**Number of positive siRNAs**
DRD1IP	7	7
RPL5	5	5
ADCK5	4	4
AKR1C2	4	4
ALS2CR8	4	4
APOBEC1	4	4
APOC2	4	4
ARCN1	4	4
ATP1A2	4	4
ATP6V0C	4	4
BID	4	4
C12orf44	4	4
C6orf103	4	4
CACNA1B	4	4
CBLN1	4	4
CD84	4	4
CEECAM1	4	4
CGB	4	4
CLCA2	4	4
CLCNKA	4	4
CLPTM1L	4	4
CUL3	4	4
DPH1	4	4
DUSP11	4	4
EMILIN3	4	4
EMP2	4	4
EPX	4	4
FABP2	4	4
FTL	4	4
GFRA2	4	4
GLS	4	4
GPC1	4	4
HNRPC	4	4
KCND1	4	4
KCNH6	4	4
KCNK13	4	4
KIR2DS3	4	4
KRT34	4	4
M6PR	4	4
MATR3	4	4
MSMB	4	4
MTA3	4	4
PCK2	4	4
PHYH	4	4
PI3	4	4
PKP1	4	4
PSG11	4	4
PSMD8	4	4

RPL10	4	4
RPL11	4	4
SLC14A1	4	4
SLC2A4	4	4
SLC6A4	4	4
SORD	4	4
TMEM134	4	4
APOA1	4	3
AQP2	4	3
AQP3	4	3
ARF1	4	3
ARRDC1	4	3
ARSK	4	3
ARVCF	4	3
ATCAY	4	3
ATP1A4	4	3
BCL2L10	4	3
C8A	4	3
CALML4	4	3
CAP1	4	3
CD33	4	3
CD99	4	3
CDH5	4	3
CG018	4	3
CGB5	4	3
CHRNE	4	3
CHRNG	4	3
CLDN14	4	3
CLDN16	4	3
CLIC1	4	3
CNN3	4	3
COLQ	4	3
COPA	4	3
COPB1	4	3
COX6A2	4	3
COX7B	4	3
CTDSP1	4	3
CXCL14	4	3
DCLRE1B	4	3
DSPP	4	3
EIF3S10	4	3
EPS8	4	3
ERN2	4	3
ETF1	4	3
F13A1	4	3
FANCD2	4	3
FAT2	4	3
FAU	4	3
FBXL11	4	3
FBXL14	4	3
FCER1G	4	3
GABRB3	4	3
GJB1	4	3

GRIA1	4	3
HAS3	4	3
HERC3	4	3
HIST1H1D	4	3
HOXB9	4	3
IL9R	4	3
KCNE1	4	3
KCNN3	4	3
KCNQ3	4	3
KISS1	4	3
KRT35	4	3
KRT36	4	3
LFNG	4	3
LILRA4	4	3
LMO3	4	3
MAT1A	4	3
MATK	4	3
MGP	4	3
MUTYH	4	3
MYH1	4	3
NACA	4	3
NDUFA8	4	3
NF2	4	3
NLRP3	4	3
NNAT	4	3
NPHP1	4	3
NR1D1	4	3
NRXN2	4	3
NY-SAR-48	4	3
OAS3	4	3
OLFM3	4	3
PELI1	4	3
PEPD	4	3
PHTF2	4	3
PIWIL1	4	3
PLCZ1	4	3
PLXNA1	4	3
PRKCZ	4	3
PRKG1	4	3
PRR8	4	3
PSMD2	4	3
PYCR1	4	3
RBBP9	4	3
RNASE2	4	3
RPL37	4	3
RPS21	4	3
RPS29	4	3
RPS3	4	3
RXRG	4	3
SARS	4	3
SCAMP4	4	3
SCAP	4	3
SIAH2	4	3

SIRT2	4	3
SLC16A1	4	3
SLC26A2	4	3
SLC2A8	4	3
SLC7A6OS	4	3
SOD3	4	3
SORBS3	4	3
SPRR3	4	3
SRRM2	4	3
STK11IP	4	3
SUPT5H	4	3
TBCB	4	3
TNN	4	3
TRPC3	4	3
TRPM1	4	3
UBA52	4	3
ACSM1	4	2
ACTL7A	4	2
ACTN4	4	2
ADCK1	4	2
ADCK2	4	2
AK3L1	4	2
AKAP5	4	2
ALKBH3	4	2
ALS2	4	2
AMELX	4	2
ANKRD13B	4	2
APOB48R	4	2
APOBEC3F	4	2
ARPC1B	4	2
ATP6V1B1	4	2
BDP1	4	2
BIRC2	4	2
BRUNOL5	4	2
BTBD10	4	2
BTBD9	4	2
C12orf50	4	2
C17orf70	4	2
C1orf25	4	2
C1QTNF4	4	2
C20orf72	4	2
C21orf124	4	2
C2orf15	4	2
C4orf36	4	2
C9orf100	4	2
CALML5	4	2
CAMK1D	4	2
CCDC134	4	2
CDC2	4	2
CHML	4	2
CLCN4	4	2
CLEC1B	4	2
COL11A2	4	2

COL1A2	4	2
COL25A1	4	2
COX17	4	2
CRYAA	4	2
CRYAB	4	2
CSRP1	4	2
CSRP3	4	2
CSTB	4	2
CYP1B1	4	2
CYP2R1	4	2
DDX55	4	2
DEPDC4	4	2
DHRS3	4	2
DKFZp434B1231	4	2
DRD3	4	2
E2F4	4	2
EFNA1	4	2
EFNB1	4	2
EIF2S1	4	2
EIF4E2	4	2
EML5	4	2
F11R	4	2
FAIM	4	2
FANCC	4	2
FBXL5	4	2
FCGR2B	4	2
FCRLA	4	2
FOXN4	4	2
FPGT	4	2
GP1BA	4	2
GPR142	4	2
GRID2	4	2
HDAC10	4	2
HHIP	4	2
HIST1H3E	4	2
HLA-B	4	2
HMCN1	4	2
HSPA9	4	2
HSPD1	4	2
IFNB1	4	2
IFNW1	4	2
IGFBP2	4	2
IL18BP	4	2
INE1	4	2
ITGA10	4	2
ITGA2	4	2
KCNK3	4	2
KIAA1217	4	2
KIAA1467	4	2
KIAA1543	4	2
KIAA1641	4	2
KIF5A	4	2
KIR3DL1	4	2

KLRB1	4	2
KRT71	4	2
KRT8	4	2
L2HGDH	4	2
LLGL1	4	2
LOC124220	4	2
LOC144742	4	2
LOC161247	4	2
LOR	4	2
LRGUK	4	2
LRRC44	4	2
MGC10981	4	2
MGC16384	4	2
MRPS11	4	2
MRS2L	4	2
MTX1	4	2
MYO1E	4	2
NAPA	4	2
NDUFV3	4	2
NPAL3	4	2
NSD1	4	2
NT5C1B	4	2
NTN2L	4	2
PCDH11X	4	2
PCDH8	4	2
PER3	4	2
PKNOX2	4	2
PMS2L5	4	2
PPP1R12B	4	2
PPP2R1B	4	2
PPP5C	4	2
PRDM10	4	2
PRKAB1	4	2
PRKCDBP	4	2
PRKD2	4	2
PRKRA	4	2
PRPH	4	2
PSG1	4	2
PSMD12	4	2
PSMD14	4	2
PTEN	4	2
PTPRC	4	2
RAB30	4	2
RABL2A	4	2
RAD51L1	4	2
RAD54B	4	2
RAGE	4	2
RALGPS2	4	2
RBMY1A1	4	2
RHOBTB3	4	2
RNF31	4	2
RPL13A	4	2
RPL32	4	2

RPS14	4	2
RPS16	4	2
RPS19	4	2
RPS4X	4	2
RPS5	4	2
RPS9	4	2
SART1	4	2
SDCBP	4	2
SHARPIN	4	2
SLC25A12	4	2
SLC4A4	4	2
SMAD5	4	2
STX2	4	2
TAC3	4	2
TAPBP	4	2
TMEM132C	4	2
TMEM132E	4	2
TMEM44	4	2
UAP1L1	4	2
USP52	4	2
WHDC1	4	2
ZFP62	4	2
ZNF512B	4	2
ZNF641	4	2
ACCN5	4	1
ACLY	4	1
ADK	4	1
ALDH18A1	4	1
ARNT2	4	1
ATPIF1	4	1
BBS9	4	1
BICC1	4	1
BNIP2	4	1
C10orf76	4	1
C10orf83	4	1
C14orf172	4	1
C14orf83	4	1
C17orf64	4	1
C18orf17	4	1
C18orf37	4	1
C19orf22	4	1
C21orf100	4	1
C2orf43	4	1
C3orf25	4	1
C6orf70	4	1
C8orf42	4	1
CABYR	4	1
CACNA2D4	4	1
CCDC114	4	1
CD4	4	1
CD8B	4	1
CDGAP	4	1
CDH24	4	1

CHST10	4	1
CIDEC	4	1
CIT	4	1
CKAP2L	4	1
CLDN9	4	1
CMIP	4	1
CNKSR3	4	1
COG6	4	1
COL9A1	4	1
CRIPT	4	1
CYP2U1	4	1
DCUN1D5	4	1
DHX32	4	1
DKFZP434P211	4	1
DKK4	4	1
DNER	4	1
DOK2	4	1
DYX1C1	4	1
EGFL9	4	1
EIF2S3	4	1
ERAF	4	1
ERBB2IP	4	1
ERG	4	1
ERGIC2	4	1
EXOC3L2	4	1
FAM3B	4	1
FAM79A	4	1
FANCA	4	1
FAT3	4	1
FGF21	4	1
FLJ14397	4	1
FLJ20209	4	1
FLJ22795	4	1
FMNL3	4	1
FRY	4	1
GPR135	4	1
GPR137	4	1
GRHL3	4	1
GYLTL1B	4	1
HIST1H4E	4	1
HLA-G	4	1
HSPC105	4	1
IL10RB	4	1
ISG20L1	4	1
ITGA3	4	1
ITGAM	4	1
KIAA0492	4	1
KIAA1618	4	1
KIF17	4	1
KL	4	1
LASS5	4	1
LOC113386	4	1
LOC126536	4	1

LOC126661	4	1
LOC144097	4	1
LOC90826	4	1
LOC91461	4	1
LOC92345	4	1
LSR	4	1
LYRM4	4	1
LYZL4	4	1
MFAP5	4	1
MFSD7	4	1
MGC29891	4	1
MICAL1	4	1
MITD1	4	1
MOGAT1	4	1
MTHFSD	4	1
MYH8	4	1
MYL9	4	1
NLGN2	4	1
N-PAC	4	1
NRXN1	4	1
NTN1	4	1
NTNG2	4	1
NUSAP1	4	1
OTOP2	4	1
PAPSS1	4	1
PARD6A	4	1
PCBP2	4	1
PIGM	4	1
PNLIPRP3	4	1
PPAP2C	4	1
PPP1R14D	4	1
PPP2R5C	4	1
PRDX2	4	1
PREX1	4	1
PRKCSH	4	1
PROK1	4	1
PSMB3	4	1
PTDSS2	4	1
PTPN4	4	1
RAET1L	4	1
RAN	4	1
RASL10A	4	1
RGAG1	4	1
RGD1310773_predicted	4	1
RPL14	4	1
RPL37A	4	1
RPS12	4	1
S100A9	4	1
SAR1A	4	1
SBEM	4	1
SETMAR	4	1
SH2D4A	4	1

SH3BP5L	4	1
SHKBP1	4	1
SHOC2	4	1
SHROOM2	4	1
SIAE	4	1
SLC16A3	4	1
SLC17A1	4	1
SLC22A9	4	1
SLC2A12	4	1
SLC6A12	4	1
SLC6A7	4	1
SLIT2	4	1
SLIT3	4	1
SMURF2	4	1
SOCS6	4	1
SOX17	4	1
SURF6	4	1
SYN2	4	1
SYT7	4	1
TBRG1	4	1
TDG	4	1
TGM7	4	1
THBS4	4	1
THOC5	4	1
TIGD7	4	1
TIMM10	4	1
TM4SF19	4	1
TMEM112B	4	1
TMEM163	4	1
TMEM168	4	1
TMEM169	4	1
TMEM170	4	1
TMEM45B	4	1
TMEM55A	4	1
TMEM67	4	1
TMPO	4	1
TPP2	4	1
TSC22D4	4	1
UBOX5	4	1
UPK1B	4	1
UTP15	4	1
VPS37D	4	1
WDR19	4	1
WDR73	4	1
WDR85	4	1
WFDC8	4	1
ZBTB7A	4	1
ZNF18	4	1
ZNF57	4	1
ZSWIM4	4	1
VPS25	4	1

Table S2. Biological function pathways enriched in the RNAi screening		
Ingenuity Canonical Pathways	-log(p-value)	Positive hits enclosed in the category
Tight Junction Signaling	4.26E+00	F11R,PARD6A,PPP2R1B,CLDN16,MYH1,PPP2R5C,PRKCZ,MYL9,CLDN14,MYH8,CNKSR3,LLGL1,PTEN,CLDN9
Caveolar-mediated Endocytosis Signaling	3.19E+00	ITGA3,ARCN1,ITGAM,COPA,ITGA10,COPB1,HLA-B,ITGA2
Calcium Signaling	2.24E+00	GRIA1,CHRNG,MYL9,TRPC3,CHRNE,CAMK1D,MYH8,HDAC10,MYH1,AKAP5,CALML5
Cellular Effects of Sildenafil (Viagra)	2.15E+00	KCNN3,MYL9,KCNQ3,PRKG1,PLCZ1,MYH8,MYH1,PPP1R12B,CALML5
Cdc42 Signaling	2.11E+00	PRKCZ,HLA-G,FCER1G,ITGA3,MYL9,PARD6A,HLA-B,ITGA2,LLGL1,ARPC1B
Stilbene, Coumarine and Lignin Biosynthesis	1.91E+00	PRDX2,KL,EPX
Cell Cycle Regulation by BTG Family Proteins	1.91E+00	HOXB9,PPP2R1B,PPP2R5C,E2F4
Amyotrophic Lateral Sclerosis Signaling	1.84E+00	GRIA1,PRPH,BIRC2,ALS2,GRID2,PROK1,BID
Role of BRCA1 in DNA Damage Response	1.83E+00	C17orf70,FANCA,FANCC,FANCD2,E2F4
Glutamate Receptor Signaling	1.80E+00	GRIA1,SLC17A1,GRID2,GLS,CALML5
Protein Ubiquitination Pathway	1.73E+00	HSPD1,PAN2,BIRC2,CRYAA,PSMD14,PSMD12,CRYAB,PSMD8,SMURF2,HLA-B,PSMD2,PSMB3,HSPA9
Regulation of eIF4 and p70S6K Signaling	1.71E+00	PRKCZ,ITGA3,EIF2S3,PPP2R1B,EIF2S1,ITGA2,PPP2R5C
Neuregulin Signaling	1.57E+00	PRKCZ,ITGA3,ERBB2IP,MATK,ITGA2,PTEN
Communication between Innate and Adaptive Immune Cells	1.51E+00	HLA-G,FCER1G,CD8B,IFNB1,CD4,HLA-B
Hereditary Breast Cancer Signaling	1.49E+00	C17orf70,FANCA,FANCC,HDAC10,FANCD2,CDK1,PTEN
PI3K/AKT Signaling	1.45E+00	PRKCZ,ITGA3,PPP2R1B,HLA-B,ITGA2,PPP2R5C,PTEN
Intrinsic Prothrombin Activation Pathway	1.38E+00	COL1A2,COL11A2,F13A1
Dopamine Receptor Signaling	1.37E+00	PPP2R1B,PPP1R14D,CALY,PPP2R5C,DRD3
Neuropathic Pain Signaling In Dorsal Horn Neurons	1.34E+00	PRKCZ,GRIA1,KCNN3,KCNQ3,CAMK1D,PLCZ1
Axonal Guidance Signaling	1.31E+00	SLIT2,EFNB1,NTN3,PROK1,NTN1,PRKCZ,EFNA1,HHIP,ITGA3,MYL9,SDCBP,MICAL1,ITGA2,SLIT3,ARPC1B,PLXNA1
Actin Cytoskeleton Signaling	1.29E+00	ITGA3,MYL9,MYH8,FGF21,ACTN4,MATK,ITGA2,MYH1,PPP1R12B,ARPC1B